

Article

An Intensity Tensor and Electric Field Gradient Tensor for Fe³⁺ at M1 Sites of Aegirine–Augite Using Single-Crystal Mössbauer Spectroscopy

Keiji Shinoda ^{1,*} and Yasuhiro Kobayashi ²¹ Graduate School of Science, Osaka Metropolitan University, Osaka 558-8585, Japan² Institute for Integrated Radiation and Nuclear Science, Kyoto University, Osaka 590-0494, Japan; kobayashi.yasuhiro.3x@kyoto-u.ac.jp

* Correspondence: shinodakeiji@omu.ac.jp

Abstract: An intensity tensor of quadrupole doublets and an electric field gradient tensor for Fe³⁺ at M1 sites in aegirine–augite ((Ca_{0.16}Na_{0.86})_{Σ1.02}(Mg_{0.13}Fe²⁺_{0.04}Fe³⁺_{0.72}Al_{0.07})_{Σ0.96}Si_{2.01}O₆) are determined using single-crystal Mössbauer spectroscopy. The components of the intensity tensor are $I_{XX} = 0.670$ (19), $I_{YY} = 0.353$ (14), $I_{XY} = -0.113$ (37) and $I_{ZZ} = 0.477$ (33). The components of the electric field gradient tensor (V_{XX} , V_{YY} and V_{ZZ}) for Fe³⁺ at M1 sites in aegirine–augite are -5.96×10^9 , -4.65×10^{10} and 5.23×10^{10} C/m³, respectively. Comparisons of the intensity tensor of aegirine–augite with those of aegirine and augite (Wo₄₀En₄₅Fs₁₆) that have already been reported and the I_{XX} , I_{YY} , I_{XY} and I_{ZZ} intensity tensor components of aegirine–augite in this study are almost the same as those of aegirine, but different from those of augite. While the M2 sites of aegirine–augite and aegirine are fully occupied with Na⁺ and Ca²⁺ ions, the M2 sites of augite are not fully occupied with Ca²⁺. The compositional dependency of the intensity tensor components suggests that the intensity tensor components for Fe³⁺ at the M1 site of a solid solution between aegirine and augite are dependent on the occupancy of large cations such as Ca²⁺ and Na⁺ at M2 sites.

Keywords: Mössbauer spectroscopy; intensity tensor; electric field gradient tensor; aegirine–augite; compositional dependence of intensity tensor



Citation: Shinoda, K.; Kobayashi, Y. An Intensity Tensor and Electric Field Gradient Tensor for Fe³⁺ at M1 Sites of Aegirine–Augite Using Single-Crystal Mössbauer Spectroscopy. *Minerals* **2023**, *13*, 1452. <https://doi.org/10.3390/min13111452>

Academic Editor: Michael Oshtrakh

Received: 17 October 2023

Revised: 16 November 2023

Accepted: 16 November 2023

Published: 18 November 2023



Copyright: © 2023 by the authors. Licensee MDPI, Basel, Switzerland. This article is an open access article distributed under the terms and conditions of the Creative Commons Attribution (CC BY) license (<https://creativecommons.org/licenses/by/4.0/>).

1. Introduction

1.1. Review of an Intensity Tensor for Fe Ions at M Sites of Pyroxene

⁵⁷Fe Mössbauer spectroscopy is a common and unique γ -ray spectroscopy technique for the analysis of Fe valence in minerals and the site occupancy of Fe in multi-site minerals. Powdered samples have generally been used for Mössbauer measurements. Although the powder method is the prevailing simple method, it is not used for the spot analyses of mineral thin sections. Several Mössbauer microspectroscopic methods have been suggested for the analysis of selected areas in thin sections ([1–4]). Mitsui et al. (2004) [3] designed a scanning-type synchrotron radiation Mössbauer microscope that attained a focused probe as small as 20 μ m in diameter using a high-resolution monochromator, a multilayer X-ray focusing mirror and a pinhole slit. Shinoda and Kobayashi [4] constructed a Mössbauer microspectrometer using a multi-capillary X-ray (MCX) lens. The focused beam size with the MCX lens was 500 μ m in diameter for 14.4 keV γ -rays. The Mössbauer spectrum of ⁵⁷Fe foil using the MCX lens was equivalent to that without the MCX lens. Although the MCX lens was confirmed to work well to focus γ -rays and was valid for the measurement of Mössbauer spectra, the intensity of the beam transmitted through the MCX lens was not very intense. A microscope can be equipped using a microspectrometer to observe samples and select measurement spots. Removal of the MCX lens allows this optical system to be modified into a Mössbauer microspectrometer for the analysis of thin sections using a pinhole as small as 300 μ m in diameter. It is thus expected that the Mössbauer

spectroscopic study of minerals could be focused on the microspectroscopic study of thin sections rather than powdered samples due to improvements in the analytical instruments. While Mössbauer microspectroscopy using the thin section of a single crystal has an advantage for spot analyses, there is an analytical problem for the Mössbauer spectra of single crystals, especially for multi-site solid solution minerals such as pyroxenes.

Pyroxene group minerals are typical multi-site solid solutions of which the structural formula is $(M2)(M1)(Si,Al)_2O_6$. In a solid solution of aegirine and augite, the $M1$ sites are almost regular octahedral sites for smaller cations such as Mg^{2+} , and the $M2$ sites are larger and distorted 8-fold sites for larger cations such as Ca^{2+} and Na^+ , while Fe^{2+} ions occupy both $M1$ and $M2$ sites [5]. Fe ions that occupy M sites show doublets in the Mössbauer spectra due to quadrupole splitting (Δ). According to Dyar et al. (2013) [6], Fe^{2+} at $M1$ sites exhibits a wide Δ (2.0–2.6 mm/s) while Fe^{2+} at $M2$ sites exhibits a narrow Δ (1.7–2.1 mm/s). Isomer shifts (δ) due to Fe^{2+} at $M1$ and $M2$ sites are commonly 1.13–1.19 mm/s. Fe^{3+} has a narrower Δ (0.3–0.7 mm/s) than Fe^{2+} . For pyroxene, in which Fe^{2+} ions are distributed in both M sites, the wide and narrow doublets are overlapped. Dyar et al. (2013) [6] determined Mössbauer hyperfine parameters (δ , Δ) for Fe^{2+} at the $M1$ and $M2$ sites of Ca-Mg-Fe pyroxenes in the pyroxene quadrilateral. These parameters provide reliable peak separation of quadrupole doublets for powdered pyroxene samples because the intensities of the quadrupole doublet can be assumed to be equal for the powdered samples. Therefore, quadrupole doublets for powdered samples are generally characterized by three parameters, i.e., δ , Δ and line width (Γ). On the other hand, intensities for the quadrupole doublet of a single crystal are not always equal. The intensity ratio of two peaks of a single crystal varies by changing the angle between the incident γ -ray direction and the crystallographic orientation of the single-crystal pyroxene ([7–9]). The orientational dependence of the intensity ratio of quadrupole doublets is a basic and important property for peak separation of overlapping wide and narrow doublets in the Mössbauer spectrum of a single crystal.

Zimmermann (1975) [10] suggested that reduced intensity (I) is favorable to express the intensity ratio of quadrupole doublets of single crystals as follows:

$$I = \frac{I^h}{I^h + I^l}, \quad (1)$$

where I^h and I^l are the intensities of the higher- and lower-Doppler-velocity components, respectively. The reduced intensity (I) is the intensity of the higher-Doppler-velocity component normalized with respect to the total intensity ($I^h + I^l$). Therefore, four parameters, δ , Δ , Γ and I , characterize the quadrupole doublet of a single crystal. Fe ions in pyroxenes show quadrupole doublets with slightly different Δ , depending on the M sites. In some cases, distinguishable doublets occur due to differences in the next-nearest-neighbor ions around the Fe ions in hedenbergite–ferrosilite pyroxenes [11]. Therefore, it is possible there is a case where the raw Mössbauer spectral data of pyroxene minerals consist of several overlapping doublets. If the reduced intensities of the doublets that comprise a thin section are known, then the intensity ratios of several doublets can be fixed during peak separation. Reduced intensity (I) is thus a necessary and important parameter for the reliable peak separation of raw Mössbauer spectral data from a single-crystal pyroxene thin section. The reduced intensity (I) is calculated from an intensity tensor as proposed by Zimmermann (1975) [10].

1.2. Compositional Dependence of the Intensity Tensor for Fe Ions at M Sites of Pyroxenes

Tennant et al. (2000) [7] applied Zimmermann's method to determine the intensity tensor and electric field gradient (EFG) tensor of Fe^{2+} occupying $M1$ sites of Mg–hedenbergite from single-crystal Mössbauer spectra. Fukuyama et al. (2022) [9] also applied Zimmermann's method to determine the intensity and EFG tensors for Fe^{2+} at the $M1$ sites of diopside, augite and hedenbergite, for Fe^{2+} at the $M2$ sites of diopside and augite and for Fe^{3+} at the $M1$ sites of augite. Fukuyama et al. (2022) [9] discussed the compositional dependence of the intensity tensors for Fe^{2+} at the $M1$ sites of Ca-Mg-Fe pyroxenes alongside

the results for Mg–hedenbergite [7]. According to Fukuyama et al. (2022) [9], the intensity tensor components of quadrupole doublets show almost constant values for 50% wollastonite component (Wo₅₀) pyroxene and are independent of the ferrosilite (Fs) component. In contrast, the intensity tensor components for Wo₄₀ augite are plotted outside of the fitting lines for the tensor components of Wo₅₀ pyroxenes.

This indicates that the intensity tensor of quadrupole doublets in Mössbauer spectra due to Fe²⁺ at the M1 sites of Ca-rich pyroxene is dependent on the Wo content, but independent of the Fs content. The results reported by Fukuyama et al. [9] suggest that the components of the intensity tensor due to Fe²⁺ at the M sites in Ca-Mg-Fe clinopyroxene minerals containing equal Wo and different Fs components are almost constant. However, this compositional dependence has not been examined in pyroxene group minerals apart from the Ca-Mg-Fe clinopyroxenes with Wo₅₀ [9].

Aegirine–augite is accepted as an independent species and is a solid solution of which the chemical composition ranges $0.2 < Q/(Q + Ae) < 0.8$ and $0.5 < Ae/(Ae + Jd)$, where Q is the sum of the Wo, enstatite (En) and Fs components, and Ae and Jd are the aegirine and jadeite components, respectively [12]. Aegirine–augite belongs to a monoclinic crystal system with space group C2/c, and shows a solid solution between aegirine (NaFe³⁺Si₂O₆) and augite ((CaMgFe²⁺)Si₂O₆) via the main replacement of NaFe³⁺ ⇌ Ca(Mg, Fe²⁺) [5]. Shinoda and Kobayashi (2019) [8] revealed the intensity tensor for Fe³⁺ at the M1 sites of Ca-free aegirine using single-crystal Mössbauer spectroscopy measurements. Fukuyama et al. (2022) [9] calculated the intensity tensor for Fe³⁺ at the M1 sites in augite (Wo₄₀En₄₅Fs₁₆). The compositional dependence of the intensity tensor for Fe³⁺ at the M1 sites of a solid solution of aegirine and augite with the replacement of NaFe³⁺ ⇌ Ca(Mg, Fe²⁺) is unknown.

In this study, the use of Zimmermann's method [10,13] to determine the intensity tensor is reviewed and applied to determine the intensity tensor for Fe³⁺ at the M1 sites of aegirine–augite. Single crystals of aegirine–augite from Tormiq, Pakistan, were used for this study. As shown later, this aegirine–augite contains 0.16 mol% Ca and 0.13 mol% Mg for six oxygens; therefore, this is an aegirine–augite. Three crystallographically oriented thin sections were prepared for X-ray diffraction measurements using Laue and precession cameras. Nine Mössbauer spectra of oriented thin sections were measured for aegirine–augite to obtain the intensity tensors of the quadrupole doublets for Fe³⁺ at the M1 sites. The components of the intensity tensor of aegirine–augite are compared with the intensity tensors of aegirine [8] and augite [9] to confirm the compositional dependence of the intensity tensor by replacing Na⁺ with Ca²⁺.

1.3. Review of the Electric Field Gradient Tensor for Fe Ions at M Sites in C2/c Pyroxene

In this section, a formulation to constrain the components of the EFG tensor using symmetrical consideration is reviewed as indicated in Ref. [8]. Aegirine–augite belongs to the space group C2/c. The M sites of aegirine–augite are located at a *special* position on a diad rotation axis along the *b*-axis [14]. The quadrupole doublet is due to an EFG tensor property that results from a point charge *q* around a Mössbauer nucleus. Assuming that the position of the Mössbauer nucleus and the position of the point charge *q* are at (0, 0, 0) and (*x*, *y*, *z*), respectively, the components (*V*_{*ij*}) of the EFG tensor *V* due to *q* are as follows:

$$V_{ij} = -q(3x_i x_j - r^2 \delta_{ij}) / r^5, \quad (2)$$

where *i, j* = 1–3, *x*₁ = *x*, *x*₂ = *y*, *x*₃ = *z*, $r = \sqrt{x^2 + y^2 + z^2}$, *d*_{*ij*} = 1 if *i* = *j* and *d*_{*ij*} = 0 if *i* ≠ *j* [15].

Assuming an M site at (0, 0, 0) and a charge *q*₁ at (*x*, *y*, *z*), an identical charge *q*₂ can be assumed at (\bar{x} , \bar{y} , *z*) from the symmetry. Detailed components (*V*¹_{*ij*}) of the EFG tensor due to *q*₁ are expressed in Equation (2), as follows:

$$\left. \begin{aligned} V_{xx}^1 &= -q(3x^2 - r^2) / r^5, & V_{yy}^1 &= -q(3y^2 - r^2) / r^5, & V_{zz}^1 &= -q(3z^2 - r^2) / r^5 \\ V_{xy}^1 &= V_{yx}^1 = -3qxy / r^5, & V_{yz}^1 &= V_{zy}^1 = -3qyz / r^5, & V_{xz}^1 &= V_{zx}^1 = -3qxz / r^5 \end{aligned} \right\} \quad (3)$$

In the same way, the components (V'^2_{ij}) of the EFG tensor due to q_2 are as follows:

$$\left. \begin{aligned} V'^2_{xx} &= -q(3x^2 - r^2)/r^5, & V'^2_{yy} &= -q(3y^2 - r^2)/r^5, & V'^2_{zz} &= -q(3z^2 - r^2)/r^5 \\ V'^2_{xy} &= V'^2_{yx} = -3qxy/r^5, & V'^2_{yz} &= V'^2_{zy} = 3qyz/r^5, & V'^2_{xz} &= V'^2_{zx} = 3qxz/r^5 \end{aligned} \right\} \quad (4)$$

Summing V'^1_{ij} of Equation (3) and V'^2_{ij} of Equation (4), V_{xz} and V_{yz} result in zero; therefore, the EFG tensor of the M site (V) is given as:

$$V = \begin{pmatrix} V_{xx} & V_{xy} & 0 \\ V_{xy} & V_{yy} & 0 \\ 0 & 0 & V_{zz} \end{pmatrix}, \quad (5)$$

where the trace of the matrix is zero ($V_{xx} + V_{yy} + V_{zz} = 0$), as known from Equation (2).

1.4. Review of Zimmermann’s Method to Determine Intensity and EFG Tensors, and Application to Fe Ions at M Sites in Aegirine–Augite

According to Zimmermann (1983) [13], the reduced intensity $I(\theta, \phi)$ of quadrupole doublets can be calculated from Equation (6) by setting a rectangular coordinate ($X Y Z$) in a crystal as:

$$I(\theta, \phi) = (e_X \ e_Y \ e_Z) \begin{pmatrix} I_{XX} & I_{XY} & I_{XZ} \\ I_{XY} & I_{YY} & I_{YZ} \\ I_{XZ} & I_{YZ} & I_{ZZ} \end{pmatrix} \begin{pmatrix} e_X \\ e_Y \\ e_Z \end{pmatrix}, \quad (6)$$

where

$$\begin{pmatrix} I_{XX} & I_{XY} & I_{XZ} \\ I_{XY} & I_{YY} & I_{YZ} \\ I_{XZ} & I_{YZ} & I_{ZZ} \end{pmatrix} \quad (7)$$

is the intensity tensor (I). The angles θ and ϕ in Equation (6) are the polar angles for the rectangular coordinates of the incident γ -rays, $I(\theta, \phi)$ is the reduced intensity and $e_X = (\sin\theta\cos\phi)$, $e_Y = (\sin\theta\sin\phi)$ and $e_Z = (\cos\theta)$ are the directional cosines of the incident γ -rays. In this study, the rectangular coordinate ($X Y Z$) is set as $X // c^*$, $Y // a$, $Z // b^*$, which is the same setting as used in Refs. [8,9]. a, b, c are the real lattice vectors and a^*, b^*, c^* are reciprocal lattice vectors of aegirine–augite.

The intensity tensor components I_{ij} and the EFG tensor components V_{ij} are related as:

$$I_{ij} = \frac{1}{2} \delta_{ij} \pm \frac{eQ}{8|\Delta|} V_{ij}, \quad (8)$$

where e is the positive elementary charge, Q is the nuclear quadrupole moment and Δ is the quadrupole splitting. The positive and negative terms correspond to the higher and lower Doppler velocities of a quadrupole doublet, respectively [10]. From Equations (5), (7) and (8), the intensity tensor I for Fe ions at M sites in aegirine–augite can be expressed as:

$$I = \begin{pmatrix} I_{XX} & I_{XY} & 0 \\ I_{XY} & I_{YY} & 0 \\ 0 & 0 & I_{ZZ} \end{pmatrix}, \quad (9)$$

where $I_{XX} + I_{YY} + I_{ZZ} = 3/2$. Therefore, the reduced intensity of a quadrupole doublet for a single crystal of aegirine–augite can be calculated from the intensity tensor modified from Equation (6):

$$I(\theta, \phi) = (e_X \ e_Y \ e_Z) \begin{pmatrix} I_{XX} & I_{XY} & 0 \\ I_{XY} & I_{YY} & 0 \\ 0 & 0 & I_{ZZ} \end{pmatrix} \begin{pmatrix} e_X \\ e_Y \\ e_Z \end{pmatrix}. \quad (10)$$

From Equation (10), an observation equation for the least-squares method (LSQ) is given as:

$$(\sin^2\theta_i\cos^2\phi_i - \cos^2\theta_i)I_{XX} + (\sin^2\theta_i\sin^2\phi_i - \cos^2\theta_i)I_{YY} + 2(\sin^2\theta_i\cos\phi_i\sin\phi_i)I_{XY} = I_i^h(\theta_i, \phi_i) - \frac{3}{2}\cos^2\theta_i, \quad (11)$$

where the index i represents the number of measurements, so that θ_i and ϕ_i are the angles of incident γ -rays for the i -th measurements. Equation (11) indicates that the intensity tensor components can be determined using multi-measurements of reduced intensity by varying the direction of the γ -rays against the crystallographic axes. By setting a_i, b_i, c_i and m_i as:

$$\left. \begin{aligned} a_i &= \sin^2\theta_i\cos^2\phi_i - \cos^2\theta_i \\ b_i &= \sin^2\theta_i\sin^2\phi_i - \cos^2\theta_i \\ c_i &= 2(\sin^2\theta_i\cos\phi_i\sin\phi_i) \\ m_i &= I_i^h(\theta_i, \phi_i) - \frac{3}{2}\cos^2\theta_i \end{aligned} \right\}, \quad (12)$$

simultaneous equations are given as follows:

$$\left. \begin{aligned} (\Sigma a_i a_i)I_{XX} + (\Sigma a_i b_i)I_{YY} + (\Sigma a_i c_i)I_{XY} &= (\Sigma a_i m_i) \\ (\Sigma a_i b_i)I_{XX} + (\Sigma b_i b_i)I_{YY} + (\Sigma b_i c_i)I_{XY} &= (\Sigma b_i m_i) \\ (\Sigma a_i c_i)I_{XX} + (\Sigma b_i c_i)I_{YY} + (\Sigma c_i c_i)I_{XY} &= (\Sigma c_i m_i) \end{aligned} \right\}. \quad (13)$$

The most probable values of the components (I_{ij}) of the intensity tensor are obtained by solving Equation (13).

A traceless intensity tensor T is derived as $T_{ij} = I_{ij} - (1/2)d_{ij}$ from Equation (8) for the higher Doppler velocity peak, which is proportional to the EFG tensor as:

$$T_{ij} = \frac{eQ}{8|\Delta|} V_{ij}. \quad (14)$$

The traceless tensor T is proportional to the EFG tensor V , and must be scaled as:

$$I_{\Delta} = 16 \left\{ T_{ZZ}^2 + \frac{1}{3}(T_{XX} - T_{YY})^2 + \frac{4}{3}(T_{XY}^2 + T_{XZ}^2 + T_{YZ}^2) \right\} = 1. \quad (15)$$

T'_{ij} obtained from $I_{ij} - (1/2)d_{ij}$, is not yet scaled; therefore, T'_{ij} must be scaled by

$$I'_{\Delta} = 16 \left\{ T'^2_{ZZ} + \frac{1}{3}(T'_{XX} - T'_{YY})^2 + \frac{4}{3}(T'^2_{XY} + T'^2_{XZ} + T'^2_{YZ}) \right\} \quad (16)$$

as follows:

$$T_{ij} = \sqrt{1/I'_{\Delta}} T'_{ij}. \quad (17)$$

T_{ij} are the components of the scaled traceless tensor T that are proportional to V (Equation (14)). T in italic font is the traceless intensity tensor before the diagonalization of the matrix. The traceless tensor T is diagonalized with the Euler angle matrix U

$$U = \begin{pmatrix} \cos\varphi & -\sin\varphi & 0 \\ \sin\varphi & \cos\varphi & 0 \\ 0 & 0 & 1 \end{pmatrix}, \quad (18)$$

as follows:

$$T = U^{-1}TU = \begin{pmatrix} T_{XX} & 0 & 0 \\ 0 & T_{YY} & 0 \\ 0 & 0 & T_{ZZ} \end{pmatrix}. \quad (19)$$

T in normal font is the traceless intensity tensor after the diagonalization of the matrix.

The orientations of the principal axes of the EFG tensor are determined from the Euler angle (φ). The maximum, minimum and intermediate terms for the absolute values are

chosen as V_{ZZ} , V_{XX} and V_{YY} among T_{XX} , T_{YY} and T_{ZZ} . The asymmetric parameter η is obtained as $\eta = (V_{XX} - V_{YY})/V_{ZZ}$. Quadrupole splitting Δ in SI units is expressed as:

$$\Delta = \frac{1}{2}eQ\frac{V_{ZZ}}{4\pi\epsilon_0}\sqrt{1 + \frac{1}{3}\eta^2}, \quad (20)$$

so that the EFG components [V_{XX} , V_{YY} and V_{ZZ} (C/m^3)] can be calculated using a Δ of $1 \text{ mm/s} = 4.80 \times 10^{-8} \text{ (eV)} = 7.69 \times 10^{-27} \text{ (J)}$, $Q = 0.16 \text{ barn}$ ($1 \text{ barn} = 10^{-28} \text{ m}^2$) [16] and $e_0 = 8.854 \times 10^{-12} \text{ (F/m)}$, the permittivity in a vacuum and the experimentally determined η (asymmetric parameter) and Δ (mm/s).

2. Materials and Methods

2.1. Chemical Analyses

A natural aegirine–augite from Tormiq, Pakistan, was used for this study. The chemical composition of the aegirine–augite was measured using scanning electron microscopy (JSM-5500, JEOL, Akishima, Japan) with energy-dispersive X-ray spectroscopy (EDAX, Pleasanton, CA, USA) at 20 kV and 500 pA. All backscattered electron images of the aegirine–augite were homogeneous. This indicates that the examined aegirine–augite does not include microstructure such as intergrowth lamellae.

2.2. X-ray Diffraction Measurements with Back Laue and Precession X-ray Cameras

A back-reflection Laue camera (Rigaku, Akishima, Japan) was used to evaluate the crystallographically oriented thin sections. Figure 1 shows an imaging plate (IP) image of back Laue X-ray diffraction for a 10 mm^3 volume of aegirine–augite using a Mo X-ray tube. A dental IP scanner (CS7600, Carestream Dental LLC, Atlanta, GA, USA) was used to scan the X-ray diffraction patterns. The size of the IP card was $57 \times 76 \text{ mm}^2$. Two IP cards were used for each exposure. The distance between a crystal and the IP was 35 mm and the X-ray exposure time was 20 min. A Laue analysis system (Norm Engineering Co., Tama, Tokyo, Japan) [17] was applied for Laue diffraction in backscatter geometry. Figure 1 shows a back-reflection Laue image of aegirine–augite fixed on a goniometer, where the b^* -axis was adjusted to be parallel to the incident X-rays, and the c^* -axis was adjusted to the vertical direction, as indicated by the arrows. From the relationship between the real and reciprocal lattices, the direction of the a -axis is the horizontal direction of Figure 1. The dial rotation axis of the goniometer is the vertical direction of Figure 1. Oriented thin sections were made in the same way as that reported in Ref. [9] as follows. By rotating the crystal with the dial rotation at 90° , the a -axis turns to the incident X-ray direction. After fixing a stick to the crystal parallel to the X-ray direction, the crystal is removed from the goniometer and then fixed on a slide glass with resin to orient the a -axis perpendicular to the slide glass. The crystal fixed on the slide glass is cut using a low-speed diamond wheel cutter and the cut plane is polished. The cut plane of the crystal is fixed on a slide glass using adhesive. The crystal is cut again and the second cut plane is polished. The adhesive is then dissolved using acetone to recover the oriented thin section. Three crystallographically oriented thin sections perpendicular to the a -, b - and c -axes were prepared for single-crystal Mössbauer spectra measurements.

The oriented thin sections were mounted on goniometers to adjust the crystallographic orientation. A Buerger precession X-ray camera (Rigaku, Akishima, Japan) was used to adjust the crystallographic axes. Figure 2 shows a Buerger precession photograph of aegirine–augite perpendicular to the b^* -axis, with the a^* -axis adjusted to the vertical direction of the X-ray precession photograph, and the c^* -axis is indicated by an arrow. Figure 2 was acquired without a K_β -removal filter. Paired spots are due to intense K_α and medium K_β radiation and radially distributed weak lines are due to white X-rays. Figure 2 indicates that this aegirine–augite is a single crystal. The distance between the crystal and X-ray film was 60 mm. The size of the X-ray film is $100 \times 100 \text{ mm}^2$. The X-ray exposure time was 4 h. The thin section mounted on a goniometer can be rotated 360°

along the horizontal axis (c -axis in this case). The goniometer with the oriented thin section can be mounted again on a Mössbauer microspectrometer with the same dial axis as the X-ray precession camera. Three thin sections perpendicular to the a -, b - and c - axes were prepared for single-crystal Mössbauer spectroscopic measurements. The thicknesses of the thin sections perpendicular to the a , b and c axes were 443, 357 and 380 μm , respectively.

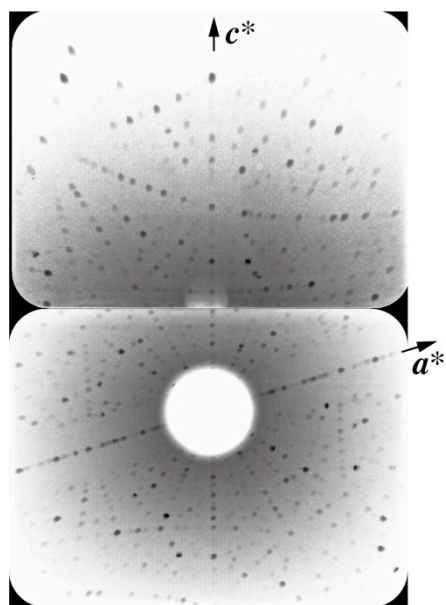


Figure 1. X-ray back-reflection Laue IP image of aegirine–augite obtained using an Mo X-ray tube. The b^* -axis is normal to the image.

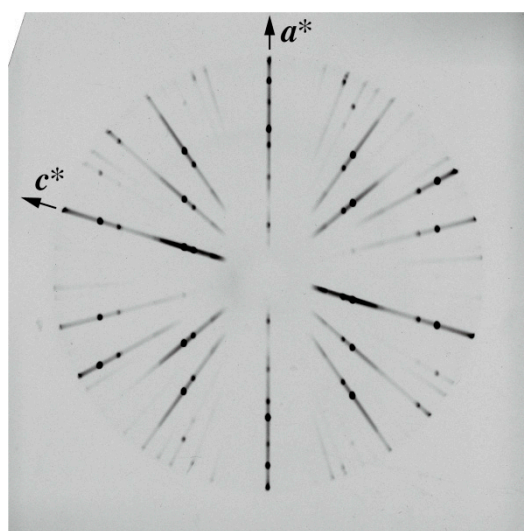


Figure 2. X-ray precession photograph of aegirine–augite obtained using an Mo X-ray tube. The b^* -axis is perpendicular to the photograph. The dial axis of the goniometer is oriented along the horizontal direction of the X-ray photograph.

2.3. Single-Crystal Mössbauer Measurements

A Mössbauer microspectrometer [4] without an MCX lens was used for this study, but instead a Pb pinhole was used to select the measurement spot. The Mössbauer spectrometer consisted of a Si-PIN semiconductor detector (XR-100CR, Amptek Inc., Bedford, MA, USA), a rotation stage to mount the goniometer with a thin section and the Pb pinhole. A $^{57}\text{Co}(\text{Rh})$ γ -ray source (RITVERC JSC, St. Petersburg, Russia) with an initial activity of

1.85×10^9 Bq and a diameter of 4 mm was used at room temperature. The Mössbauer spectra were measured in transmission mode on a constant-acceleration spectrometer with a 1024-channel multichannel analyzer. The two mirror spectra were folded at the 512.5th channel for measurements No 1-3 and 7-9, and at the 513.0th for measurements No 4-6. The data points were modified to 512 channels using mathematical interpolation. Mössbauer measurements were performed in two periods for No 1-3 and 7-9 and for No 4-6, and different velocity driving systems were used in the two periods. The different folding points result from the different velocity driving systems. The velocity range was ± 5 mm/s. The velocity was calibrated with respect to the spectrum for an ^{57}Fe -enriched α -iron foil of 2 μm thickness, that was covered with Kapton foil, before measuring nine spectra. The measurement time was in the range of 46.5 to 66.5 h for all Mössbauer spectra. The signal-to-noise ratios (I/\sqrt{N}) , where I is the maximal intensity of the absorption peak and N is the average number of counts at the non-resonant part of the spectrum, were in the range of 25 to 71. Residuals, which are the differences between the calculated and experimental spectra, are shown at the bottom of spectra.

The MossWinn program was used for peak separation and transmission integral correction to compensate for the sample thickness (MossWinn, 2018) [18]. To estimate the source line width for transmission integral correction, the line width of the third and fourth peaks in the magnetic sextet of the reference absorber hematite powder mixed with boron nitride powder with a thickness of 25 mg Fe/cm^2 was determined as 0.24 mm/s. This broadening of the experimental natural line, which is 0.19 mm/s for ^{57}Fe , indicates contributions of the instrumental line broadening and thickness effects from both the source and reference absorber. Then, we suggested that the obtained experimental line broadening can be roughly considered as the result of the only source line broadening up to 0.147 mm/s. This value was further used for the Mössbauer spectra fits using a transmission integral.

The average values of δ , Δ and Γ for Fe^{3+} at M1 sites in aegirine–augite after transmission integral correction were 0.39, 0.34 and 0.11 mm/s, respectively. The normalized statistical quality of the fit, χ^2 , will also be shown in the Section 3. The transmission integral correction using MossWinn results in the relative intensity of the higher- and lower-Doppler-velocity components of the doublets. Therefore, only reduced intensities will be shown in the Section 3.

Figure 3a shows a schematic diagram of the goniometer arrangement on the rotation stage, a thin section fixed on the goniometer (G), the Pb pinhole, the γ -ray source (γ), the Si-PIN detector (Si) and an objective lens for optical observation (L). Figure 3b shows a photograph of a thin section fixed on a goniometer (C), a Si-PIN semiconductor detector and an objective lens mounted on the Mössbauer spectrometer. The detector and the objective lens are mounted on a mechanical stage. By shifting the objective lens to the front of the sample, the positions of the pinhole and the sample can be confirmed. After selecting a measuring spot on the pinhole position, the detector is put back to the sample position for Mössbauer measurements. Nine Mössbauer spectra of the oriented aegirine–augite thin sections were collected by setting the dial angles at the adjusted angle using X-ray measurement and with modification of the angles $\pm 30^\circ$ from the adjusted angle for each thin section. Figure 3c shows schematic diagrams on the modifying orientations of the thin section at the adjusted angle and at an angle of 30° by rotating the goniometer. The thin sections were flat plates. The areas of the flat plates were larger than the pinhole. One thin section was used to measure the Mössbauer spectra for three orientations of the γ -ray. The first orientation of the γ -ray is perpendicular to the thin section. Therefore, the γ -ray path length indicated by light blue arrows is the thickness of the thin section. The second and the third orientations of the γ -ray were inclined from the perpendicular direction of the thin section with angles of $\pm 30^\circ$, which were attained by rotating the goniometer using a dial axis. Therefore, the γ -ray path length is multiplied by $1/\cos 30^\circ$.

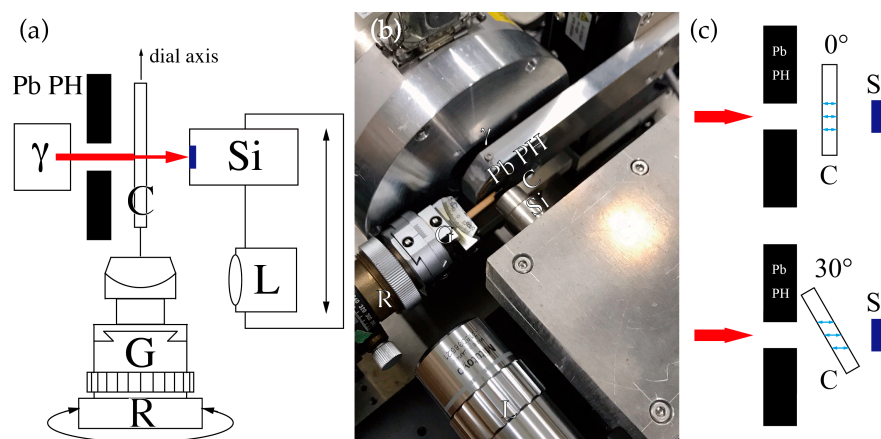


Figure 3. (a) Vertical view of schematic diagram of the goniometer setting on the Mössbauer spectrometer. γ : γ -ray propagation direction; Pb PH: lead pinhole; G: goniometer; C: oriented thin section adjusted on the goniometer; Si: Si-PIN detector; R: rotation stage of the horizontally rotating axis; L: optical lens. (b) Photograph of goniometer set on the Mössbauer spectrometer. (c) Horizontal view of schematic diagrams on modifying orientations of the thin section at the adjusted angle and at the angle of 30° by rotating goniometer.

3. Results and Discussion

3.1. Chemical Analyses

Table 1 shows the results of the chemical analyses of aegirine–augite. The weight percentages (wt%) given for the oxides are the average of 10 measurement points. Estimated errors are given in parentheses. As shown using the Mössbauer spectra in the next section, the ferrous and ferric ion contents were 5.2% and 94.8%, respectively. FeO was used as a Fe standard; therefore, the weight percent of FeO was divided into 1.29% for ferrous and 23.54% for ferric ions. The weight percent of Fe_2O_3 was calculated from the correction as $(159.70/71.85)/2 \times 23.54\%$, where 159.70 and 71.85 are the molecular weights of Fe_2O_3 and FeO, respectively. The chemical formula of this crystal was calculated as $(\text{Ca}_{0.16}\text{Na}_{0.86})_{\Sigma 1.02}(\text{Mg}_{0.13}\text{Fe}^{2+}_{0.04}\text{Fe}^{3+}_{0.72}\text{Al}_{0.07})_{\Sigma 0.96}\text{Si}_{2.01}\text{O}_6$, which indicates that the total positive charge is 11.96 and is almost equal to 12.00. The sum of the Wo and En components was 0.33 mol% and the ratio of $\text{Al}^{3+}/\text{Fe}^{3+} = \text{jadite/aegirine} = 0.10$; therefore, this is aegirine–augite according to the nomenclature of pyroxenes [12].

Table 1. Chemical analyses of aegirine–augite.

Oxides	wt%
SiO_2	54.86 (21)
Al_2O_3	1.65 (5)
FeO	24.83 (22)
(FeO)	(1.29 (1))
(Fe_2O_3)	(26.15 (23))
MgO	2.38 (12)
CaO	4.08 (23)
NaO	12.10 (16)
total	102.65
Formulae (O = 6)	molar ratio
Si	2.01
Al	0.07
Fe^{2+}	0.04
Fe^{3+}	0.72
Mg	0.13
Ca	0.16
Na	0.86

3.2. Mössbauer Spectroscopic Analyses of Aegirine–Augite Single Crystal

3.2.1. Mössbauer Spectra of Oriented Aegirine–Augite Thin Sections

The black dot data points in Figure 4a–c are the raw Mössbauer spectra data of aegirine–augite for the γ -ray // *a*-, *b*- and *c*-axes, respectively. Nine spectra commonly show intense quadrupole splitting doublets as narrow as 0.33 mm/s and weak peaks at approximately 2.0 and 2.5 mm/s. The intense doublet is due to Fe³⁺ at the M1 sites. The two weak peaks are due to the higher-Doppler-velocity components of Fe²⁺ at the M sites. Amthauer and Rossman (1984) [19] observed two weak peaks at approximately 2.5 mm/s and 1.9 mm/s in the Mössbauer spectra of aegirine–augite measured at room temperature and assigned the former to Fe²⁺ at the M1 sites and the latter as also due to Fe²⁺ at the M1 sites (written as Fe^{“2+”} in Ref. [19]) with a different type of next-nearest neighbor arrangement, e.g., Ca²⁺ instead of Na⁺. To resolve the raw data of aegirine–augite into three doublets, the parameters of δ , Δ and Γ for Fe²⁺ and Fe^{“2+”} at M1 sites in Ref. [19] were assumed to be $\delta = 1.15$ and 1.08 mm/s, $\Delta = 2.77$ and 1.81 mm/s and $\Gamma = 0.31$ and 0.60 mm/s, respectively. The peak intensity ratios of these doublets for nine different directions of incident γ -rays were calculated from the intensity tensor of hedenbergite in Ref. [9]. The assumed intensity tensor for the two types of Fe²⁺ at M1 sites is

$$I_{\text{Fe}^{2+}(\text{M1})\text{Hd}} = \begin{pmatrix} 0.370 & 0.019 & 0 \\ 0.019 & 0.467 & 0 \\ 0 & 0 & 0.663 \end{pmatrix} \quad (34 \text{ in Ref. [9]})$$

For example, I for Fe²⁺ at the M1 sites of $i = 1$ in this study is calculated as 0.467 from Equation (34) in Ref. [9]; therefore, $I^1: I^h$ is assumed to be 0.533:0.467.

The nine Mössbauer spectra consist of intense doublets due to Fe³⁺ at the M1 sites where two peaks of a doublet are overlapping. These overlapping intense absorption peaks of the raw spectra were considered to be a modified Lorentzian function. To correct the intensity of the absorption peaks, thickness corrections of the raw spectra were performed using the MossWinn program and the transmission integral method [18]. A procedure for thickness correction adopted for aegirine [8] was repeated here. The effective thickness (t) was calculated according to the following formula, as in Ref. [8]

$$t = d\rho \frac{w}{100} \frac{N_A}{A} a\sigma_0 f' , \quad (21)$$

where d is the sample thickness in centimeters, ρ is the density of the aegirine–augite (3.5 g/cm³), w is the weight percent of Fe, N_A is Avogadro’s constant, A is the atomic weight of Fe, a is the fractional abundance of ⁵⁷Fe (0.022), σ_0 is the resonant cross-section of Mössbauer nuclei (206.4×10^{-20}) and f' is the recoilless fraction of the source, which is 0.874 for aegirine [20].

Figure 4 shows the raw data and results of peak separation after transmission integral correction using the MossWinn program [18]. The green, blue and red doublets are due to Fe³⁺ at the M1 sites, Fe²⁺ at the M1 sites and Fe^{“2+”} at the M1 sites, respectively. According to Ref. [18], the colored doublets are ideal spectra that do not include a thickness effect. The black lines are the total fitting lines obtained via the summation of the three colored spectra after including the thickness effect.

Table 2 shows the γ -ray directions of the i -th measurement, sample thickness (d), effective thickness (t) calculated from Equation (21), I for Fe²⁺ at the M1 sites calculated from Equation (34) in Ref. [9], area ratio of doublets for Fe²⁺ at the M1 and Fe³⁺ at the M1 sites, reduced intensities (I) due to Fe³⁺ at the M1 sites after transmission integral correction [18] and δ , Δ and Γ for Fe³⁺ at the M1 sites. The averaged area ratio of doublets for the two types of Fe²⁺ at the M1 sites and Fe³⁺ at the M1 sites are 2.3 (2)%, 2.9 (10)% and 94.8 (10)%, respectively. This suggests that aegirine–augite includes 5.2% ferrous ions and 94.8% ferric ions.

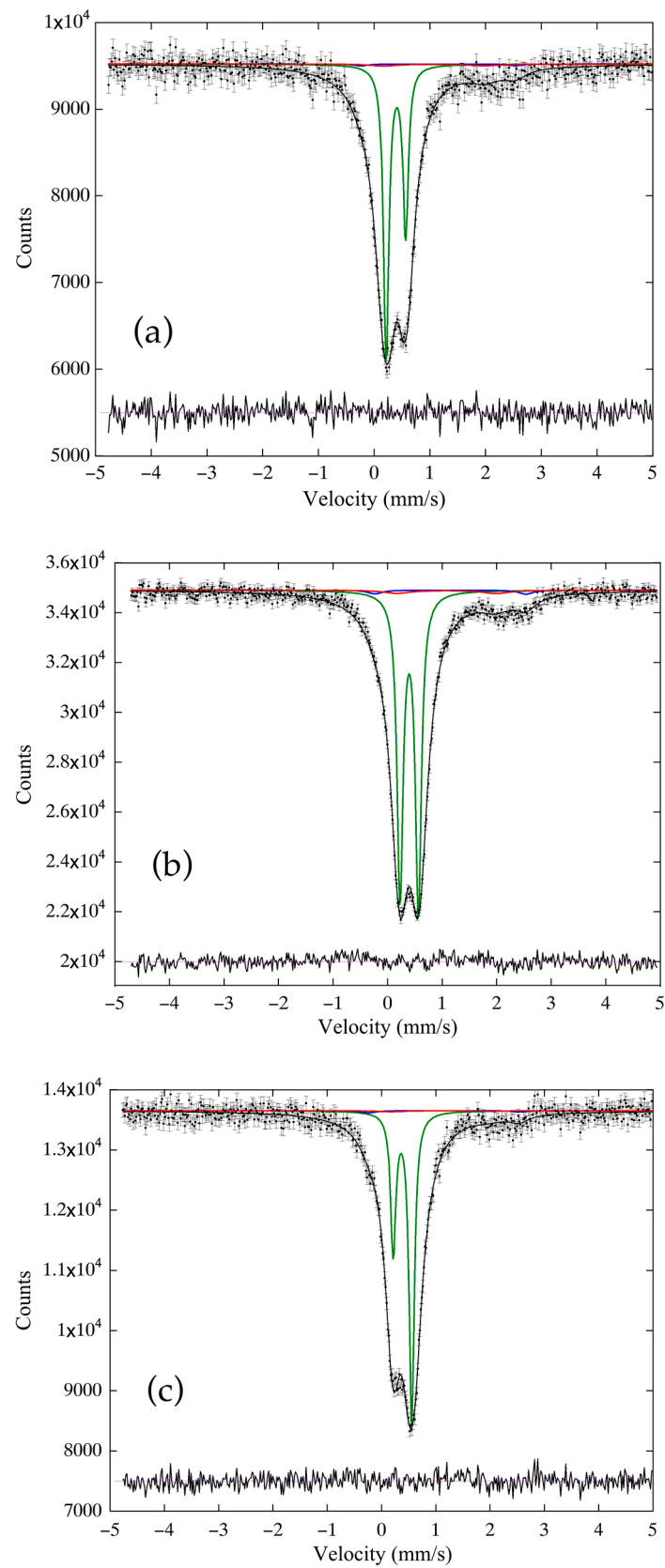


Figure 4. Mössbauer spectra of oriented aegirine-augite thin sections under (a) $\gamma // Y(a)$, (b) $\gamma // Z(b^*)$ and (c) $\gamma // c$.

Table 2. γ -ray directions, sample thickness (d), effective thickness (t), area ratio (%) of ferrous and ferric Fe ions, reduced intensities (I) and ^{57}Fe Mössbauer parameters of the doublets for Fe^{3+} at M1 sites of aegirine–augite.

Oriented Thin Section i	#1 \perp a ($d = 443 \mu\text{m}$)			#2 \perp b ($d = 357 \mu\text{m}$)			#3 \perp c ($d = 380 \mu\text{m}$)		
	1	2	3	4	5	6	7	8	9
	γ -ray direction and effective thickness (t)								
θ ($^\circ$)	90	60	120	180	150	150	90	60	120
ϕ ($^\circ$)	90	90	90	0	73	253	343	343	343
γ -ray effective thickness (t)	// $Y(a)$ 12.5		14.4	// $Z(b)$ 10.0		11.6	// c 10.7		12.3
	Calculated I for Fe^{2+} at M1 from Equation (34) in [9]								
Fe^{2+} at M1	0.467	0.516	0.516	0.663	0.615	0.615	0.368	0.442	0.442
	Doublet area ratio (%)								
Fe^{2+} at M1	1.8	2.4	2.5	2.7	2.3	2.1	2.0	2.4	2.8
Fe^{2+} at M1	4.0	4.4	2.9	4.3	3.8	3.6	1.8	0.7	0.4
Fe^{3+} at M1	94.2	93.3	94.6	93.0	93.9	94.3	96.2	96.9	96.7
	I for Fe^{3+} at M1 site								
$I = I^h / (I^l + I^h)$	0.366	0.391	0.360	0.509	0.413	0.404	0.690	0.623	0.678
	^{57}Fe Mössbauer parameters								
δ (mm/s)	0.39	0.39	0.40	0.40	0.40	0.40	0.39	0.39	0.38
Δ (mm/s)	0.35	0.35	0.35	0.34	0.34	0.35	0.34	0.34	0.34
Γ (mm/s)	0.11	0.11	0.10	0.13	0.11	0.12	0.11	0.10	0.11
Normalized χ^2	1.001	1.024	1.018	1.289	1.008	1.033	0.987	1.072	1.076

3.2.2. Calculation of Intensity Tensor and EFG Tensor for Fe^{3+} at M1 Sites of Aegirine–Augite Using the Zimmermann Method

I_i , θ_i and ϕ_i in Table 2 were applied to Equation (13) to calculate the intensity tensor for aegirine–augite. The most probable components of an intensity tensor for aegirine–augite are:

$$I_{\text{Fe}^{3+}(\text{M1})\text{Agt}} = \begin{pmatrix} 0.670(19) & -0.113(37) & 0 \\ -0.113(37) & 0.353(14) & 0 \\ 0 & 0 & 0.477(33) \end{pmatrix}, \quad (22)$$

where the errors are given in parentheses. Note that aegirine–augite is shortened to Agt after symbols for rock-forming minerals [21].

The EFG tensor is calculated from the intensity tensor (Equation (22)) by applying Equations (14)–(19) as follows. The traceless intensity tensor T' and its components T'_{ij} are set, so that T' is given as:

$$T'_{\text{Fe}^{3+}(\text{M1})\text{Agt}} = \begin{pmatrix} 0.170 & -0.113 & 0 \\ -0.113 & -0.147 & 0 \\ 0 & 0 & -0.023 \end{pmatrix}. \quad (23)$$

The T' components are applied to Equation (16), by which I'_D is calculated as $I'_\Delta = 0.705$. Scaling T'_{ij} using I'_Δ gives the traceless intensity tensor T as:

$$T_{\text{Fe}^{3+}(\text{M1})\text{Agt}} = \begin{pmatrix} 0.188 & -0.125 & 0 \\ -0.125 & -0.162 & 0 \\ 0 & 0 & -0.026 \end{pmatrix}. \quad (24)$$

Diagonalization of T using the Euler angle matrix U ,

$$U_{\text{Fe}^{3+}(\text{M1})\text{Agt}} = \begin{pmatrix} \cos(-17.8^\circ) & -\sin(-17.8^\circ) & 0 \\ \sin(-17.8^\circ) & \cos(-17.8^\circ) & 0 \\ 0 & 0 & 1 \end{pmatrix} \quad (25)$$

gives a diagonalized traceless intensity tensor T :

$$T_{\text{Fe}^{3+}(\text{M1})\text{Agt}} = U_{(25)}^{-1} T_{(24)} U_{(25)} = \begin{pmatrix} 0.228 & 0 & 0 \\ 0 & -0.203 & 0 \\ 0 & 0 & -0.026 \end{pmatrix}. \quad (26)$$

The diagonalized tensor T (Equation (26)) is proportional to the EFG tensor V , as indicated in Equation (14). The three components of V (V_{XX} , V_{YY} and V_{ZZ}) are defined to be ordered as $|V_{XX}| \leq |V_{YY}| \leq |V_{ZZ}|$. The component -0.026 in Equation (26) is the minimum absolute value; therefore, T_{ZZ} corresponds to V_{XX} , and the V_{XX} axis of the EFG tensor is oriented along the Z -axis. In the same way, the maximum absolute value T_{XX} and the intermediate absolute value T_{YY} correspond to V_{ZZ} and V_{YY} , respectively. The asymmetry parameter η is determined as $\eta = (V_{XX} - V_{YY})/V_{ZZ} = 0.776$. Substituting $\Delta = 0.34$ mm/s and η into Equation (20) gives the EFG component V_{ZZ} as 5.23×10^{10} C/m³, so that V_{XX} and V_{YY} are -5.96×10^9 and -4.65×10^{10} C/m³, respectively.

3.2.3. Compositional Dependence of the Intensity Tensor for Fe³⁺ at M1 Sites between Aegirine and Augite Solid Solution

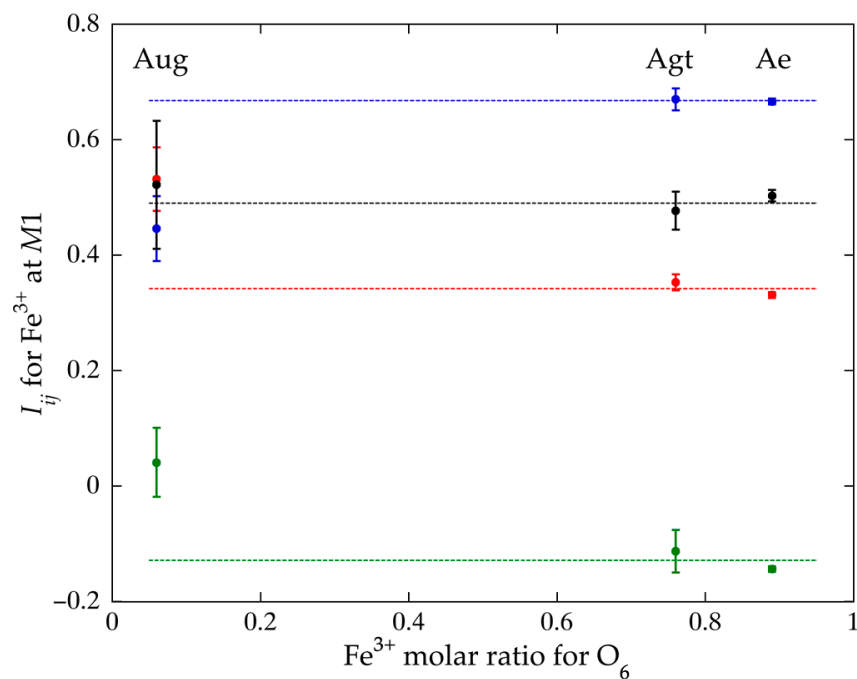
To confirm the compositional dependence of the intensity tensor for Fe³⁺ at the M1 sites between aegirine and augite solid solution, the intensity tensors for aegirine (*Ae*) and augite (Wo₄₀En₄₅Fs₁₆) (*Aug*) are referred from Refs. [8] and [9], respectively:

$$I_{\text{Fe}^{3+}(\text{M1})\text{Ae}} = \begin{pmatrix} 0.666(5) & -0.144(5) & 0 \\ -0.144(5) & 0.331(5) & 0 \\ 0 & 0 & 0.503(10) \end{pmatrix}, \quad (\text{Ae})$$

$$I_{\text{Fe}^{3+}(\text{M1})\text{Aug}} = \begin{pmatrix} 0.446(56) & 0.041(60) & 0 \\ 0.041(60) & 0.532(55) & 0 \\ 0 & 0 & 0.522(111) \end{pmatrix} \quad (\text{Aug})$$

The chemical compositions of aegirine and augite are Na_{1.03}(Fe³⁺_{0.89}Al_{0.04}) Σ _{0.93}Si_{2.04}O₆ [8] and (Ca_{0.75}Na_{0.03}Fe²⁺_{0.25}Fe³⁺_{0.06}Mg_{0.84}Ti_{0.02}) Σ _{1.95}(Si_{1.91}Al_{0.16}) Σ _{2.07}O₆ [9], respectively. Figure 5 shows the relationship between the Fe³⁺ molar ratio for O₆ of aegirine, aegirine–augite and augite, and the intensity components (I_{XX} , I_{YY} , I_{XY} and I_{ZZ}) for Fe³⁺ at the M1 sites extracted from Equation (22), (*Ae*) [8] and (*Aug*) [9]. The four components I_{XX} , I_{YY} , I_{XY} and I_{ZZ} of aegirine–augite are almost the same as those of aegirine. The averages of the I_{XX} , I_{YY} , I_{XY} and I_{ZZ} components for aegirine and aegirine–augite are 0.668, 0.342, -0.129 and 0.490, respectively. Broken lines in Figure 5 are average lines of the intensity tensor components for aegirine and aegirine–augite. In contrast, the intensity tensor components for augite are plotted outside of the average lines. The intensity tensor components (I_{XX} , I_{YY} , I_{XY} and I_{ZZ}) for Wo₄₀ augite deviate from the average lines for aegirine and aegirine–augite by as much as 0.2.

The molar ratios of the sum of Ca²⁺ and Na⁺ for aegirine, aegirine–augite and augite are 1.03, 1.02 and 0.78 for O₆, respectively. The chemical compositions of aegirine and aegirine–augite indicate that these M2 sites are fully occupied with Ca²⁺ and Na⁺, and that the M2 sites of augite are partially occupied with Ca²⁺ and Na⁺ up to as high as 78%. The remaining 22% of the M2 sites of augite are thus considered to be occupied with Fe²⁺.



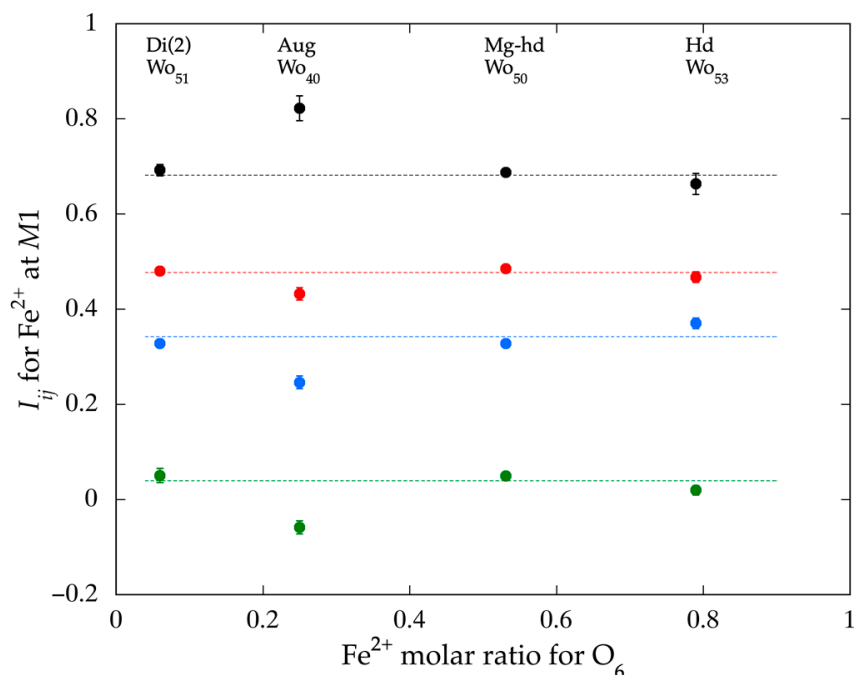


Figure 6. Relationship between the Fe²⁺ molar ratio for O₆ of diopside (2), augite, Mg–hedenbergite [7] and hedenbergite, and the intensity components for Fe²⁺ at the M1 sites modified from Fukuyama et al. (2022) [9]. I_{XX} (blue), I_{YY} (red), I_{XY} (green) and I_{ZZ} (black) are the intensity tensor components for Fe²⁺ at the M1 sites. Error bars are as low as the data point radius. The horizontal axis is modified to the Fe²⁺ molar ratio for O₆ from the Fs components. Broken lines are average lines of the intensity tensor components for diopside (2), Mg–hedenbergite [7] and hedenbergite.

Comparing Figures 5 and 6 reveals that the deviations from the average lines of the tensor components for Fe³⁺ at the M1 sites of augite are larger than those for the Fe²⁺ at the M1 sites for augite, as much as 0.1 from the average lines for Wo₅₀ Ca–Mg–Fe pyroxenes [9]. The difference in the deviation between the Ca- and Na-rich pyroxenes may be due to the difference in the valence of the Fe ions. Another possible reason for the difference is the replacement of Ca²⁺ by Na⁺ ions. The M2 sites of Wo₅₀ Ca–Mg–Fe pyroxenes can be fully occupied by Ca²⁺. The M2 sites of aegirine–augite and aegirine are almost all occupied by Na⁺, i.e., 5% larger than Ca²⁺. Larger deviations in the intensity tensor components for Fe³⁺ at the M1 sites than those for Fe²⁺ at the M1 sites may be due to the replacement of Ca²⁺ by Na⁺. The result of this study suggests that the intensity tensors for Fe²⁺ and Fe³⁺ at the M1 sites are generally dependent on the ratio of large cations such as Ca²⁺ and Na⁺ at the M2 sites.

3.2.4. Principal Axes of the EFG Tensor for Fe³⁺ at M1 Sites of Aegirine–Augite

Figure 7 shows the principal axes of the EFG tensor for Fe³⁺ at the M1 sites of aegirine–augite drawn as red lines from the Euler angle in $\mathbf{U}_{\text{Fe}^{3+}(\text{M1})\text{Agt}}$ (Equation (25)). Figure 7 indicates that the principal axes of V_{YY} and V_{ZZ} of the EFG tensor for Fe³⁺ at the M1 sites of aegirine–augite are almost parallel to the a^* - and c - axes, and suggests that the principal axes of the EFG tensor for Fe³⁺ at the M1 sites are common in aegirine–augite solid solution.

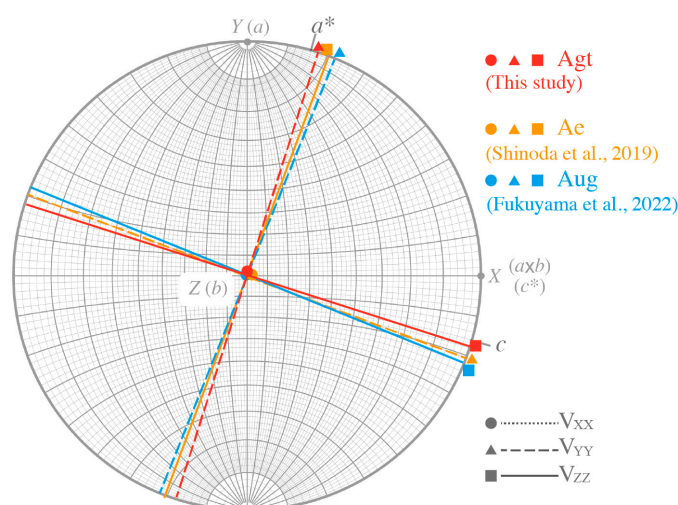


Figure 7. Principal axes of EFG tensors for Fe^{3+} at M1 sites. The principal axes of aegirine–augite are represented by red lines. The principal axes of aegirine [8] and augite [9] are represented as orange and blue lines, respectively. The V_{XX} axis is represented by circles and dotted lines, V_{YY} is represented by triangles and broken lines and V_{ZZ} is represented by squares and solid lines.

4. Conclusions

The intensity tensor of Mössbauer doublets and the EFG tensor for Fe^{3+} at the M1 sites of aegirine–augite were experimentally determined using the Mössbauer spectra of crystallographically oriented thin sections. The intensity tensor components (I_{XX} , I_{YY} , I_{XY} and I_{ZZ}) for Fe^{3+} at the M1 sites of aegirine–augite calculated from the thickness-corrected intensity of quadrupole doublets were 0.670 (19), 0.353 (14), -0.113 (37) and 0.477 (33), respectively. The EFG components (V_{XX} , V_{YY} and V_{ZZ}) of Fe^{3+} at the M1 sites in aegirine–augite were -5.96×10^9 , -4.65×10^{10} and 5.23×10^{10} C/m³, respectively. Comparison of the intensity tensor components with those of aegirine and augite indicated the intensity tensor components for Fe^{3+} at the M1 sites of aegirine–augite were dependent on the ratio of large cations such as Ca^{2+} and Na^+ at the M2 sites.

Author Contributions: Conceptualization, K.S.; methodology, K.S. and Y.K.; writing—original draft preparation, K.S. All authors have read and agreed to the published version of the manuscript.

Funding: This research was conducted at the Institute for Integrated Radiation and Nuclear Science, Kyoto University, within the Visiting Researcher Program.

Data Availability Statement: Data will be provided by authors if requested.

Acknowledgments: K.S. thanks the three anonymous reviewers and Michael Oshtrakh for critical and valuable comments that improved the manuscript.

Conflicts of Interest: The authors declare no conflict of interest.

References

1. McCammon, C.A.; Chaskar, V.; Richard, G.G. A technique for spatially resolved Mössbauer spectroscopy applied to quenched metallurgical slags. *Meas. Sci. Technol.* **1991**, *2*, 657–662. [CrossRef]
2. Yoshida, Y.; Suzuki, K.; Hayakawa, K.; Yukihiro, K.; Soejima, H. Mössbauer spectroscopic microscope. *Hyperfine Interact.* **2009**, *188*, 121–126. [CrossRef]
3. Mitsui, T.; Kobayashi, Y.; Seto, M. Development of scanning-type synchrotron radiation Mössbauer microscope using focused X-ray. *Jpn. J. Appl. Phys.* **2004**, *43*, 389–393. [CrossRef]
4. Shinoda, K.; Kobayashi, Y. Mössbauer microspectrometer with a multicapillary X-ray lens. *Jpn. Mag. Mineral. Petrol. Sci.* **2018**, *47*, 163–167, (In Japanese with English Abstract and Figure Captions). [CrossRef]
5. Deer, W.A.; Howie, R.A.; Zussman, J. Introduction. In *Rock Forming Minerals. Single Chain Silicates*; 2A; Longman: London, UK, 1978; pp. 3–18.

6. Dyar, M.D.; Klima, R.L.; Fleagle, A.; Peel, S.E. Fundamental Mössbauer parameters of synthetic Ca-Mg-Fe pyroxenes. *Am. Min.* **2013**, *98*, 1172–1186. [[CrossRef](#)]
7. Tennant, W.C.; McCammon, C.A.; Miletich, R. Electric field gradient and mean-squared-displacement tensors in hedenbergite from single-crystal Mössbauer millprobe measurements. *Phys. Chem. Miner.* **2000**, *27*, 156–163. [[CrossRef](#)]
8. Shinoda, K.; Kobayashi, Y. Determination of the electric field gradient tensor of Fe³⁺ in the M1 site of aegirine by single crystal Mössbauer spectroscopy. *J. Mineral. Petro. Sci.* **2019**, *114*, 130–141. [[CrossRef](#)]
9. Fukuyama, D.; Shinoda, K.; Takagi, D.; Kobayashi, Y. Compositional dependence of intensity and electric field gradient tensors for Fe²⁺ at the M1 site in Ca-rich pyroxene by single crystal Mössbauer spectroscopy. *J. Mineral. Petro. Sci.* **2022**, *117*, 11. [[CrossRef](#)]
10. Zimmermann, R. A method for evaluation of single crystal ⁵⁷Fe Mössbauer spectra (FeCl₂·4H₂O). *Nucl. Instrum. Methods.* **1975**, *128*, 537–543. [[CrossRef](#)]
11. Dowty, E.; Lindsley, D.H. Mössbauer spectra of synthetic hedenbergite-ferrosilite pyroxenes. *Am. Min.* **1973**, *58*, 850–868.
12. Morimoto, N. Nomenclature of pyroxenes. *Miner. J.* **1989**, *14*, 198–221. [[CrossRef](#)]
13. Zimmermann, R. The intensity tensor formulation for dipole transitions (e.g., ⁵⁷Fe) and its application to the determination of EFG tensor. In *Advances in Mössbauer Spectroscopy*; Thosar, B.V., Ed.; Elsevier Scientific Publishing Co.: Amsterdam, The Netherlands, 1983; pp. 273–315.
14. Cameron, M.; Papike, J.J. Crystal chemistry of silicate pyroxenes. In *Pyroxenes*; Prewitt, C.T., Ed.; Reviews in Mineralogy and Geochemistry 7; Mineralogical Society of America: Washington, DC, USA, 1980; pp. 5–92.
15. Travis, J.C. The electric gradient tensor. In *An Introduction to Mössbauer Spectroscopy*; May, L., Ed.; Plenum Press: New York, NY, USA, 1971; pp. 75–103.
16. Dufek, P.; Blaha, P.; Schwarz, K. Determination of the Nuclear Quadrupole Moment of ⁵⁷Fe. *Phys. Rev. Lett.* **1995**, *75*, 3545–3548. [[CrossRef](#)] [[PubMed](#)]
17. Laue Analysis Program. Norm Engineering Co. Available online: http://www.din.or.jp/~norm/sub2_e.htm (accessed on 4 August 2023).
18. MossWinn—Mossbauer Spectrum Analysis and Database Software. Available online: <http://www.mosswinn.com/> (accessed on 4 August 2023).
19. Amthauer, G.; Rossman, G.R. Mixed valence of iron on minerals with cation clusters. *Phys. Chem. Miner.* **1984**, *11*, 37–51. [[CrossRef](#)]
20. De Grave, E.; Van Alboom, A. Evaluation of ferrous and ferric Mössbauer fractions. *Phys. Chem. Miner.* **1991**, *18*, 337–342. [[CrossRef](#)]
21. Kretz, R. Symbols for rock-forming minerals. *Am. Min.* **1983**, *68*, 277–279.
22. Shannon, R.D. Revised effective ionic radii and systematic studies of interatomic distances in halides and chalcogenides. *Acta Cryst.* **1976**, *A32*, 751–767. [[CrossRef](#)]

Disclaimer/Publisher’s Note: The statements, opinions and data contained in all publications are solely those of the individual author(s) and contributor(s) and not of MDPI and/or the editor(s). MDPI and/or the editor(s) disclaim responsibility for any injury to people or property resulting from any ideas, methods, instructions or products referred to in the content.